Society For Biomaterials

Gradual pore formation in natural origin scaffolds throughout subcutaneous implantation

Ana M. Martins,[1,2,3] James D. Kretlow,[3] Ana R. Costa-Pinto,[1,2] Patrícia B. Malafaya,[1,2] Emanuel M. Fernandes,[1,2] Nuno M. Neves,[1,2] Catarina M. Alves,[1,2] Antonios G. Mikos,[3] F. Kurtis Kasper,[3] Rui L. Reis[1,2]

[1]3B's Research Group, Biomaterials, Biodegradables and Biomimetics, University of Minho, Headquarters of the European Institute of Excellence on Tissue Engineering and Regenerative Medicine, AvePark, Taipas, Guimarães 4806-909, Portugal
[2]ICVS/3B's, PT Government Associate Laboratory, Braga/Guimarães, Portugal
[3]Department of Bioengineering, Rice University, 6100 Main Street, Houston, Texas 77005-1892

Received 28 March 2011; revised 26 July 2011; accepted 1 August 2011
Published online in Wiley Online Library (wileyonlinelibrary.com). DOI: 10.1002/jbm.a.33261

Abstract: This study used a rat subcutaneous implantation model to investigate gradual *in situ* pore formation in a self-regulating degradable chitosan-based material, which comprises lysozyme incorporated into biomimetic calcium phosphate (CaP) coatings at the surface to control the scaffold degradation and subsequent pore formation. Specifically, the *in vivo* degradation of the scaffolds, the *in situ* pore formation, and the tissue response were investigated. Chitosan or chitosan/starch scaffolds were studied with and without a CaP coating in the presence or absence of lysozyme for a total of six experimental groups. Twenty-four scaffolds per group were implanted, and eight scaffolds were retrieved at each of three time points (3, 6, and 12 weeks). Harvested samples were analyzed for weight loss, microcomputed tomography, and histological analysis. All scaffolds showed pronounced weight loss and pore formation as a function of time. The highest weight loss was 29.8% ± 1.5%, obtained at week 12 for CaP chitosan/starch scaffolds with lysozyme incorporated. Moreover, all experimental groups showed a significant increase in porosity after 12 weeks. At all time points no adverse tissue reaction was observed, and as degradation increased, histological analysis showed cellular ingrowth throughout the implants. Using this innovative methodology, the ability to gradually generate pores *in situ* was clearly demonstrated *in vivo*. © 2011 Wiley Periodicals, Inc. J Biomed Mater Res Part A: 00A: 000–000, 2011.

Key Words: natural origin materials, *in vivo* degradation, enzymes, *in situ* pore formation, tissue response

How to cite this article: Martins AM, Kretlow JD, Costa-Pinto AR, Malafaya PB, Fernandes EM, Neves NM, Alves CM, Mikos AG, Kasper FK, Reis RL. 2011. Gradual pore formation in natural origin scaffolds throughout subcutaneous implantation. J Biomed Mater Res Part A 2011:00A:000–000.

INTRODUCTION

The evaluation of a bone tissue engineering constructs in an *in vivo* subcutaneous model is often the first step following *in vitro* characterization. In previous studies we proposed the use of nonporous, stimulus responsive chitosan-based scaffolds with self-regulated degradation for bone tissue engineering applications.[1,2] This approach is based on the use of a material that exhibits both self-regulated degradation and the ability for gradual *in situ* pore formation. Chitosan and starch by themselves or in combination do not have adequate bone bonding, osteoconductive or osteoinductive properties for bone tissue engineering applications, and calcium phosphate (CaP) coating may give rise to such key properties.

The incorporation of lysozyme into CaP coatings prepared at the surface of chitosan-based scaffolds using a biomimetic methodology was used previously to control and tailor the degradation rate of scaffolds and subsequent formation of pores.[2–4] The main advantage of the biomimetic method[5–7] is the use of physiological conditions (pH 7.4 at 37°C) that simulate those involved in the formation of apatite in bone.[8] Moreover, this technique allows the

Correspondence to: R. L. Reis; e-mail: rgreis@dep.uminho.pt
Contract grant sponsor: Portuguese Foundation for Science and Technology (FCT); contract grant numbers: SFRH/BPD/66897/2009, SFRH/BPD/26763/2006, SFRH/BD/24735/2005
Contract grant sponsor: European NoE EXPERTISSUES; contract grant number: NMP3-CT-2004-500283
Contract grant sponsor: National Institutes of Health; contract grant number: R01 DE17441
Contract grant sponsor: Baylor College of Medicine Medical Scientist Training Program; contract grant number: NIH T32 GM07330
Contract grant sponsor: Rice Institute of Biosciences and Bioengineering's Biotechnology Training Grant; contract grant number: NIH T32 GM008362
Contract grant sponsor: Keck Center Nanobiology Training Program of the Gulf Coast Consortia; contract grant number: 5 T90 DK070121-04

incorporation of proteins and bioactive agents into CaP coatings without compromising their activity.[2,9,10] *In vitro*, these scaffolds gradually exhibit *in situ* pore formation.[2] To prove the concept of *in situ* pore formation *in vitro*, previous studies simulating the inflammatory response were performed, and the formation of pores was clearly visible when lysozyme was incorporated in CaP chitosan scaffolds.[2] The combination of chitosan with other biodegradable materials has already been shown to be effective for bone-related applications.[11–13] The inclusion of starch in chitosan matrices constitutes an interesting approach towards obtaining scaffolds with enhanced degradation rates since starch is acting as a sacrifice material.[1] Furthermore, starch is enzymatically hydrolyzed by α-amylase, an enzyme present in blood serum. Several *in vitro* and *in vivo* studies have shown that scaffolds produced from starch-based biomaterials are biocompatible in specific applications[14–16] and biodegradable in different conditions.[1,3,17,18]

To prove the concept of *in situ* pore formation within chitosan-based scaffolds *in vivo*, a rat subcutaneous implantation model was used. It was hypothesized that using this innovative methodology, the scaffolds, which at the time of implantation exhibit very promising mechanical properties due to the absence of macroporosity,[1] will exhibit *in situ* pore formation facilitated by previously impregnated lysozyme and by enzymes present in the body (namely the α-amylase and lysozyme). This study was designed to investigate the following specific aims: (i) study the host tissue response (ii) assess the degradation of the scaffolds *in vivo*, (iii) characterize the *in situ* formation of pores, and (iv) assess *in vivo* the concept of *in situ* pore formation.

MATERIALS AND METHODS

Materials

Degradable scaffolds based on chitosan and corn starch were used. Two different compositions were prepared using a precipitation method: chitosan (CH) and chitosan/starch scaffolds (CS).[1] Briefly, chitosan was dissolved in 1% (v/v) acetic acid to obtain a 5% (w/v) solution. Then, using the same procedure, another formulation was prepared with the following ratio: 60/40 chitosan/starch. The chitosan and chitosan/starch solutions were cast into moulds and frozen (−20°C) overnight.[1] They were then immersed in a precipitation solution (25% (v) NaOH 1*M* and 75% (v) Na_2SO_4 0.5*M*)[1,19] and washed several times with distilled water. After this procedure, four other formulations were prepared based on previously used biomimetic coating techniques[2–4] consisting of an impregnation of the materials with bioactive glass called Bioglass((45S5; NOVABONE Alachua, FL) followed by an immersion in a 1× simulated body fluid (SBF, 37°C, pH 7.4) solution, which ionic concentrations are similar to those of the human blood plasma. Briefly, chitosan (CH) and chitosan/starch (CS) scaffolds were immersed in a wet bed of bioglass for 6 h on an orbital rotator. After that, the scaffolds where immersed in 1× SBF with and without lysozyme (1 g/L) for 7 days at 37°C (nucleation stage). This stage allows for the formation of CaP nuclei. After the nucleation stage, all samples were washed with distilled water and immersed in 1.5× SBF solution for 7 days at 37°C to enhance CaP nuclei growth (growth stage). Four different samples were obtained using the biomimetic coating technique: CaP chitosan scaffolds (CaPCH), CaP chitosan/starch scaffolds (CaPCS), CaP chitosan scaffolds with incorporated lysozyme (CaPCH + lysozyme), and CaP chitosan/starch scaffolds with incorporated lysozyme (CaPCS + lysozyme).[2–4] Thus, a total of six scaffold compositions were prepared: CH, CS, CaPCH, CaPCS, CaPCH + lysozyme, and CaPCS + lysozyme. All chemical reagents were purchased from Sigma (St. Louis, MO) unless otherwise specified.

Implants preparation

In this study, 5 mm diameter and approximately 1.5 mm thick scaffolds were used. All scaffolds were sterilized with ethylene oxide gas for 14 h prior to implantation in conditions described elsewhere.[20,21] One day before subcutaneous implantation surgery, the implants were prewetted with phosphate buffered saline (PBS) solution in 24-well plates overnight under sterile conditions.

Subcutaneous implantation

All animal manipulations were approved by Rice University's Institutional Animal Care and Use Committee. Twenty-four male Wistar rats 41−44 days old (Charles River Laboratories, USA) were used for subcutaneous implantation of acellular scaffolds. Three implantation periods were used: 3, 6, and 12 weeks (3W, 6W, and 12W, respectively). Anesthesia was induced with a 4% isoflurane/oxygen mixture and maintained with 2% isoflurane during surgical manipulation. The rats were monitored to ensure that an appropriate surgical plane of anesthesia was maintained. The fur on the dorsum of the rat was clipped closely prior to surgery. Then, the animals were placed in a ventral position, the clipped dorsum was disinfected with povidone-iodine, and six small longitudinal incisions were made. A pocket was bluntly dissected at each incision, and one scaffold was placed in each pocket. One implant from each experimental group was implanted in 24 rats (six implants per rat). A total of eight scaffolds per experimental group per time point were implanted. Previous studies reported successful implantation of six materials in rat dorsal subcutaneous pockets using Wistar rats of similar or lower size.[22–25] The incisions were closed with simple interrupted 5-0 Vicryl sutures. Each animal received an intraperitoneal injection of sterile saline to aid postoperative recovery (1 mL/100 g/h of anesthesia) and a subcutaneous injection of buprenorphine (0.025 mg/kg) both before and 8–12 h after surgery for analgesia. On the following day, two additional doses of subcutaneous buprenorphine (0.025 mg/kg) were injected for continued postoperative analgesia regimen (i.e., at 20–24 and 32–36 h postop). Care was taken to give all subcutaneous injections caudal to the implantation sites. Animals were housed individually with water and food given *ad libitum*. At each time point, animals were anesthetized by isoflurane inhalation and euthanized with carbon dioxide asphyxiation. The implants were retrieved after a bilateral thoracotomy was performed to ensure death.

Preparation of samples for weight loss and microcomputed tomography analysis

After each implantation time, three scaffolds from each group were decellularized prior to weight loss measurement and microcomputed tomography (μ-CT) analysis. Briefly, the scaffolds were immersed in double-distilled water (ddH_2O) and placed in a 24-well plate at −20°C. After that, scaffolds underwent three freeze/thaw cycles in liquid nitrogen and in a 37°C water bath, respectively, to disrupt attached cells and remove cellular debris.[26] Finally, scaffolds were air-dried in a laminar flow hood.

Weight loss measurements

All samples were weighed before subcutaneous implantation (initial weight). After 3, 6, and 12 weeks of implantation, three decellularized samples of each condition were dried and weighed to determine the final weight and calculate the weight loss in Eq. (1).

$$\text{Weight loss}\,(\%) = \frac{\text{Initial weight} - \text{Final weight}}{\text{Initial weight}} \qquad (1)$$

Microcomputed tomography analysis

Retrieved implants used for weight loss measurements were also used for μ-CT analysis. Three samples from each group were used as controls (i.e., nonimplanted specimens). μ-CT was carried out with a high-resolution μ-CT scanner (Skyscan 1072, Skyscan, Kontich, Belgium) using a pixel size of 5.27 μm and integration time of 1.7 ms. The X-ray source was set at 70 keV of energy and 142 μA of current. Approximately 400 projections were acquired over a rotation range of 180° with a rotation step of 0.45°. Data sets were reconstructed using standardized cone-beam reconstruction software (NRecon v1.4.3, SkyScan). The output format for each sample was 400 serial 1024 × 1024 bitmap images. Representative data sets were segmented into binary images using a dynamic threshold of 40–255 for polymer and 130–255 for CaP coating (gray values). These representative data sets were used for morphometric 3D analysis (CT Analyser, v1.5.1.5, SkyScan) and to build 3D models (ANT 3D creator, v2.4, SkyScan). The morphometric analysis included porosity and pore interconnectivity. 3D virtual models of representative regions in the bulk of the scaffolds were created, visualized, and registered using image processing software (CT Analyser and ANT 3D creator).

Thermogravimetric analysis

The same samples of different conditions used for weight loss measurements and μ-CT analysis were used for thermogravimetric analysis (TGA). The amount of inorganic component (mineral) was estimated by TGA as a function of implantation time. TGA was performed using a TGA Q 500 series thermogravimetric analyser (TA Instruments, USA), at a heating rate of 10°C/min, under a nitrogen flow of 40 ml/min and for a temperature range from 50 to 450°C. Three samples (approx. 10 mg) of each material were tested both before and after implantation (3, 6, and 12 weeks).

A typical thermogram showed two main plateaus; the first corresponds to the complete evaporation of sample moisture, and the second, to the end of organic fraction thermal degradation. We considered two temperature points (150 and 450°C) at the first derivative local minimum, one from each plateau. These temperature points were used to estimate the weight fractions of organic (chitosan or/and starch) and inorganic (mineral) components: the weight measured at 150°C corresponds to the sample dry weight, and the weight at 450°C includes both inorganic components and ashes resulting from the organic component pyrolysis.

Histology

After euthanasia, the implants were retrieved along with the surrounding tissue and processed for histology. Five specimens from each group per time point were fixed in 10% neutral buffered formalin and then dehydrated in a graded series of ethanol, immersed in infiltration solutions, embedded in Technovit glycol methacrylate (kit 8100, Heraeus Kulzer, EBSciences, USA) and subsequently polymerized. Three specimens from each group per time period were cut to obtain longitudinal sections, and two specimens were cut to obtain transverse sections of 7 μm thickness using a modified microtome equipped with a tungsten blade (Leica RM 2155).

Sections were stained with hematoxylin and eosin (H&E) to evaluate the *in vivo* degradation, pore formation, cellular infiltration throughout the implants and tissue response.

The van Gieson stain, which presents an affinity for collagen, was also used. In this case, collagen stains pinkish-red, cells brownish, and muscle stains yellow. The sections were subsequently examined under polarized light to visualize mature collagen.

For visualization of the CaP coating, additional sections were exposed to 5% silver nitrate solution under UV for 25 min and counterstained with 0.5% safranin O solution. All images were obtained using an Olympus BX61 Motorized System Microscope and attached video camera (Olympus DP70). Histological sections from all time points were scored by the authors (AMM, ARP, and CMA), blinded for group conditions and implantation time, and consensus was reached on the final score. The cellular ingrowth within the implants and the degradation of each sample was qualitatively scored based on dissolution, cracks, and fragmentation on a scale modified from De Jong, as shown in Table I.[27]

Immunohistochemistry

Further, immunohistochemical staining was performed to detect α-smooth muscle actin (α-SMA). The antibody against α-SMA (Abcam, ab5694) was used to detect blood vessels since α-SMA is one of the constituents of the vessel walls, allowing the observation of vessel ingrowth. The slides were washed with phosphate buffered saline and endogenous peroxidase was blocked with 0.6% hydrogen peroxide (H_2O_2) in methanol, at room temperature (RT) for 30 min. R.T.U. Vectastain® Universal Elite ABC Kit (Vector, VCPK-7200) was used for antibody incubation, according to the

TABLE I. Histological Grading Scale for the Degradation and Cellular Growth Within the Implants

Scoring Category	Response	Score
Cellular growth within implant	Abundance presence of cells and fibrous tissue around all fragments	4
	Marked presence of cells and/or formation of fibrous tissue around most fragments	3
	Moderate presence of cells in cracks of implant and/or formation of fibrous tissue around fragments of implant	2
	Minimal presence of cells within cracks of the implant (some cells present with or without connective tissue formation)	1
Degradation	Abundant degradation of implant with (almost) complete fragmentation	4
	Marked degradation of implant with presence of several fragments	3
	Moderate degradation of implant with cracks in implant and/or some fragments	2
	Minimal degradation of implant, some minor dissolution on edges, cracks in implant and/or small fragment present	1

instructions of the manufacturer. Briefly, sections were incubated overnight with the primary antibody (anti-α-SMA) at 4°C and humidified atmosphere. After washing with PBS solution, antibody detection was revealed by using the Peroxidase Substrate Kit DAB (Vector, VCSK-4100). Slides were washed in water for 5 min and then counterstained with Harris' hematoxylin for nuclear contrast, at RT for 2 min. After this, samples were washed with water, dehydrated in graded ethanol (50, 70, 95, and 100%), cleared with xylene, and mounted with Histofluid mounting medium (Marienfeld, Germany). All images were obtained using an Olympus BX61 Motorized System Microscope and attached video camera (Olympus DP70).

Statistics

Results of weight loss and μ-CT analysis are expressed as means ± standard deviation with $n = 3$ for each group. Results of histological scoring are expressed as means ± standard deviation with $n = 5$ for each group. Single factor analysis of variance (ANOVA) was used to determine statistical significance within a data set. If ANOVA detected a significant difference within the data set, Tukey's honestly significantly different (HSD) multiple comparison test was used to determine significant differences between groups and conditions. All tests were conducted with a confidence interval of 95% ($p < 0.05$).

RESULTS AND DISCUSSION

Weight loss measurements

Lysozyme, an enzyme ubiquitous in the human body,[28,29] has been reported to be responsible for the *in vivo* degradation of chitosan[30,31] and has been previously incorporated into and released from CaP coatings of chitosan-based scaffolds, while retaining biological activity.[2,3] As observed in Figure 1, all groups degraded gradually as a function of implantation time. A significant increase ($p < 0.05$) in weight loss was observed after 3, 6, and 12 weeks for chitosan scaffolds in the presence of lysozyme (CaPCH+lysozyme), as compared to chitosan scaffolds (CH) at the respective time points (Fig. 1). These results indicate that lysozyme has a significant effect in the biodegradation of chitosan. Statistically significant weight loss ($p < 0.05$) was observed for chitosan/starch scaffolds (CS) with and without CaP coating and both in the presence and in the absence of lysozyme (CaPCS + lysozyme and CaPCS, respectively) after 12 weeks of implantation. The highest weight loss after 12 weeks was 29.8% ± 1.5% for CaP chitosan/starch scaffolds with lysozyme incorporated (Fig. 1). It is expected that for longer

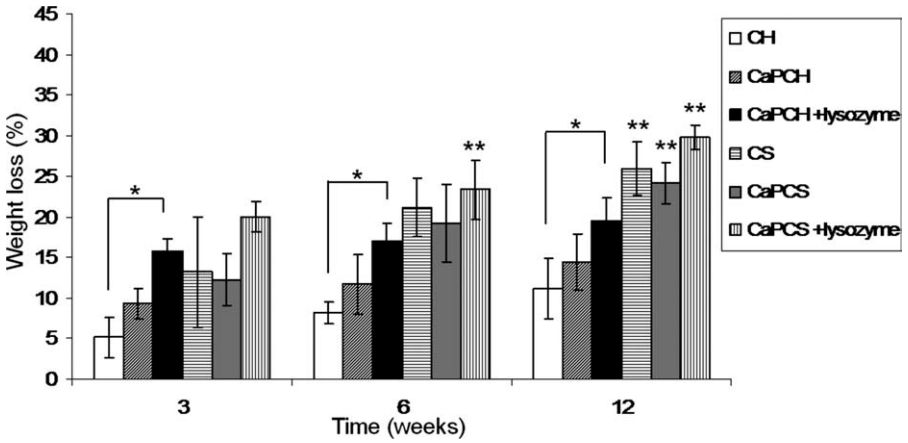

FIGURE 1. Weight loss profile of different groups after subcutaneous implantation for up to 12 weeks. Results are expressed as means ± standard deviation with $n = 3$ for each bar. (*) indicates a significant difference ($p < 0.05$) between groups at the same time point. (**) indicates a significant difference ($p < 0.05$) between the same condition at different time points.

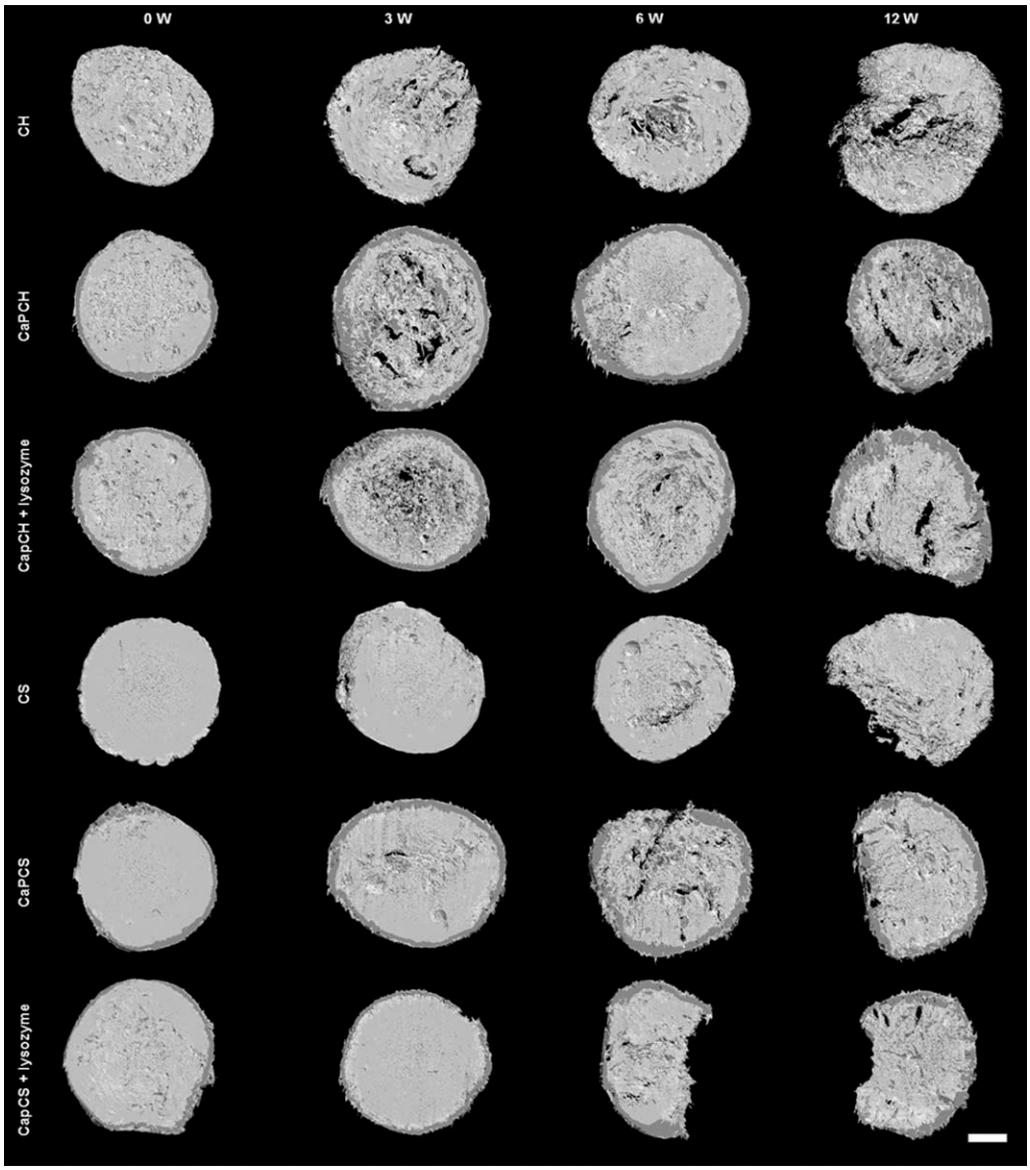

FIGURE 2. Images of chitosan-based scaffolds obtained by μ-CT: before implantation (week 0 -control) and after 3, 6, and 12 weeks of subcutaneous implantation. The scale bar is 1 mm and applies to all images.

implantation times, the degradation and the *in situ* formation of pores will be greater than that obtained in the present studies performed up to 12 weeks. Comparing all groups at the same time point, chitosan scaffolds had the lowest weight loss overall, but this was, as expected, slightly increased when lysozyme was present. Chitosan/starch scaffolds with and without CaP and in the presence or absence of lyzozyme (CS, CaPCS + lysozyme, and CaPCS, respectively) demonstrated greater weight loss than chitosan scaffolds (CH, CaPCH, and CaPCH + lysozyme) after 6 and 12 weeks (Fig. 1).

Previous studies investigated the degradation of chitosan scaffolds with and without CaP coating and in the presence and absence of lysozyme at pH 5 to simulate the inflammatory response.[2] The weight loss *in vitro* was not as pronounced as that observed *in vivo*. Similar to the *in vivo* experiments described herein, *in vitro* CaP coated chitosan scaffolds with incorporated lysozyme (CaPCH + lysozyme) had the highest weight loss.[2] However, the complete dissolution of the CaP coatings was not observed *in vivo*, although it was *in vitro* at pH 5, possibly indicating that the inflammatory response following implantation *in vivo* does not achieve such a low pH or does not sustain this low pH for as long as the previously performed *in vitro* study.[2]

This study also examined the effect of the addition of starch into the chitosan phase compared with chitosan scaffolds alone. The presence of starch in addition to chitosan seems to accelerate the degradation of scaffolds compared to that of chitosan alone (Fig. 1). Starch is degraded by α-amylase, an enzyme also present in the human body, namely in the human blood.[32] Starch granules with 5–10 μm dimensions were homogeneously distributed throughout the chitosan matrix enhancing hydrolysis by

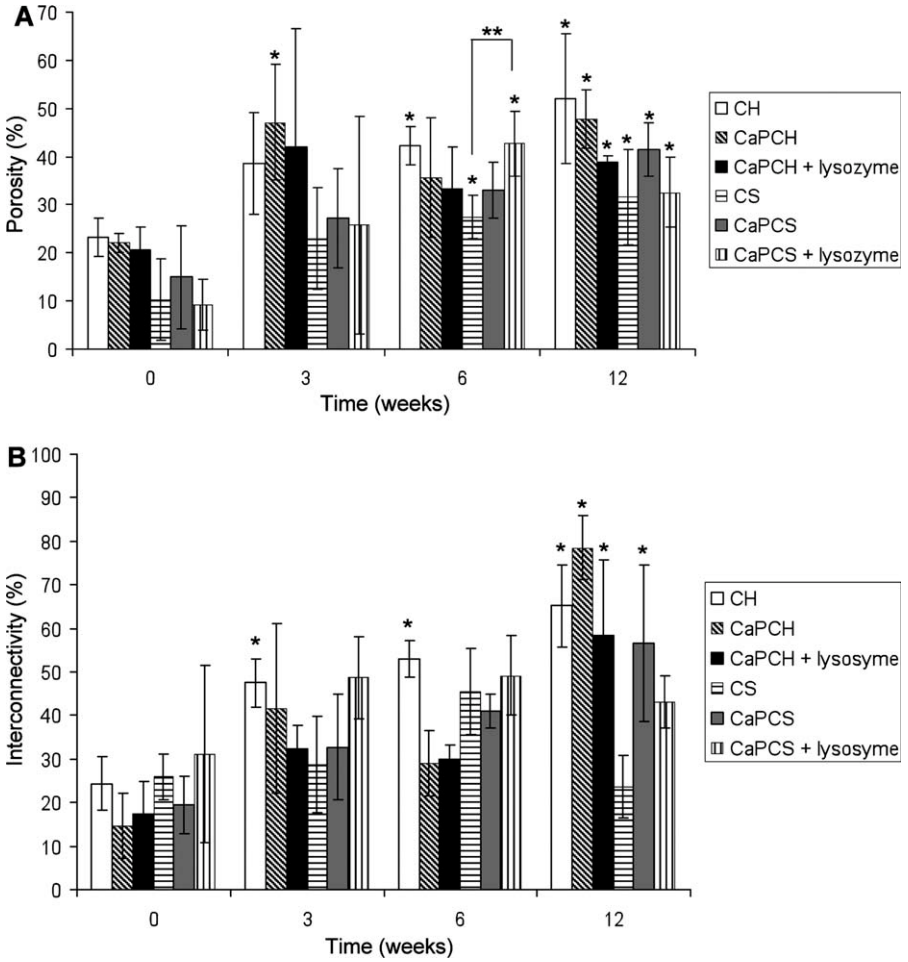

FIGURE 3. Porosity (A) and pore interconnectivity (B) of chitosan-based scaffolds before implantation (week 0 -control) and as a function of implantation time. Results are expressed as means ± standard deviation with $n = 3$ for each bar. (*) indicates a significant difference ($p < 0.05$) between groups at different time points compared with controls (0 days). (**) indicates a significant difference ($p < 0.05$) between different groups at the same time point.

enzymes existing *in vivo*, namely lysozyme and α-amylase.[1] The pore size and distribution in the scaffold are controlled by the location of the "sacrifice" phase (starch), the degradation of which increases the microporosity by the release of starch granules (small dots visible at high magnifications in Figure 4 for chitosan/starch scaffolds—CS, CaPCS, and CaPCS + lysozyme). These results are in agreement with the weight loss data (Fig. 1).

μ-CT analysis

The μ-CT analysis performed on all experimental groups showed an increase in scaffold porosity as a function of implantation time (Fig. 2). At 3-weeks postimplantation, degradation was observed in 3D images for chitosan-based formulations compared with controls (Fig. 2). After 6 weeks, results indicated increased degradation for all the materials. The trend towards an accelerated increase in porosity/degradation was observed for all conditions up to week 12 as can be observed in Figure 2. Nevertheless, analysis of the 3D images did not indicate a remarkable effect for the presence of lysozyme in chitosan scaffolds, but there did appear to be enhanced degradation after 6 and 12 weeks when lysozyme was incorporated in CaP chitosan/starch scaffolds (Fig. 2). Furthermore, the CaP coating (dark grey) was observed in 3D images at all time points for CaP coated scaffolds, indicating the aforementioned lack of coating degradation as was previously observed *in vitro*[2] (Fig. 2).

According to Figure 3(A), all groups had an increase of porosity after 3 weeks of implantation. However, no significant differences in porosity were found between groups at the same time point with the exception of CaP chitosan/starch scaffolds with incorporated lysozyme (CaPCS + lysozyme) after 6 weeks of implantation. This condition (CaPCS + lysozyme) presented significant higher porosity ($p < 0.05$) compared with chitosan/starch scaffolds (CS) (43% ± 7% and 27% ± 4%, respectively). After 6 weeks of implantation lysozyme seems to positively enhance the porosity, of chitosan/starch scaffolds corroborating the weight loss results (Fig. 1). After 3 weeks, no significant differences were found for all studied groups when compared with the porosity of the corresponding control (nonimplanted, W0) samples. However, after 6 weeks of implantation, porosity

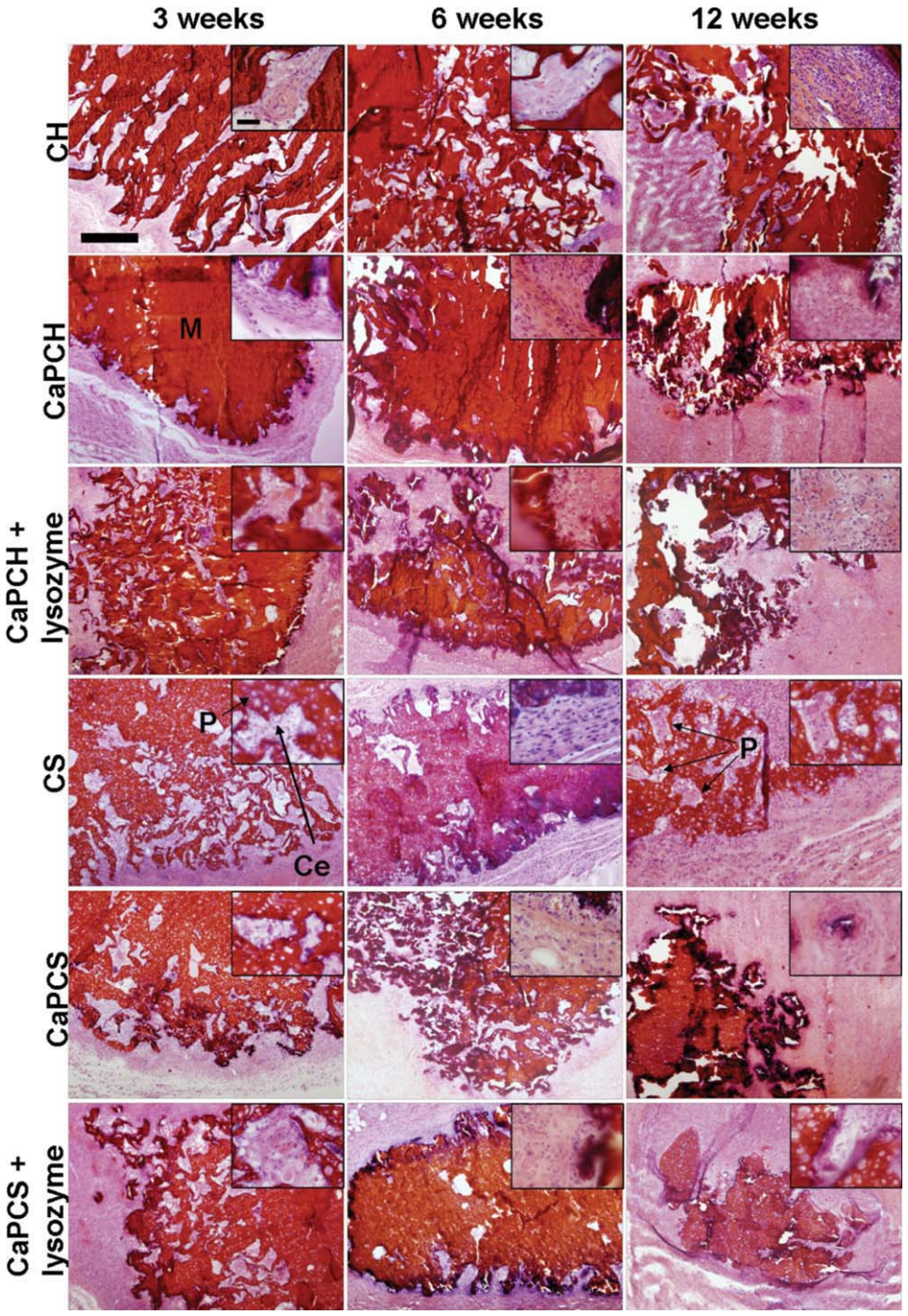

FIGURE 4. Representative histological sections of scaffolds implanted subcutaneously and stained with H&E after 3, 6, and 12 weeks. The images, showing the progressive degradation of materials accompanied by a progressive tissue ingrowth, are presented at 4× and 40× magnification. The scale bars represent 500 μm and apply to all images. Chitosan-based scaffolds (M) appear in red. Pores (P) appear filled by cells (Ce) in pink or blue. [Color figure can be viewed in the online issue, which is available at wileyonlinelibrary.com.]

significantly increased for chitosan (CH), chitosan/starch (CS), and CaP chitosan/starch scaffolds with incorporated lysozyme (CaPCS + lysozyme) [Fig. 3(A)], relative to the respective W0 controls. The same trend was observed after 12 weeks of implantation, showing significantly higher porosity for all scaffolds compared to that of control samples. These results indicate that all groups have the ability to form pores *in situ* as a function of implantation time. All groups presented a significant increase in porosity over time that was further enhanced by the presence of lysozyme. In the absence of lysozyme, CS scaffolds presented an increase of 22% of porosity over 12 weeks of implantation (initial porosity of 10% ± 8% increased to 32% ± 10%), while the porosity of CaPCS + lysozyme scaffolds increased

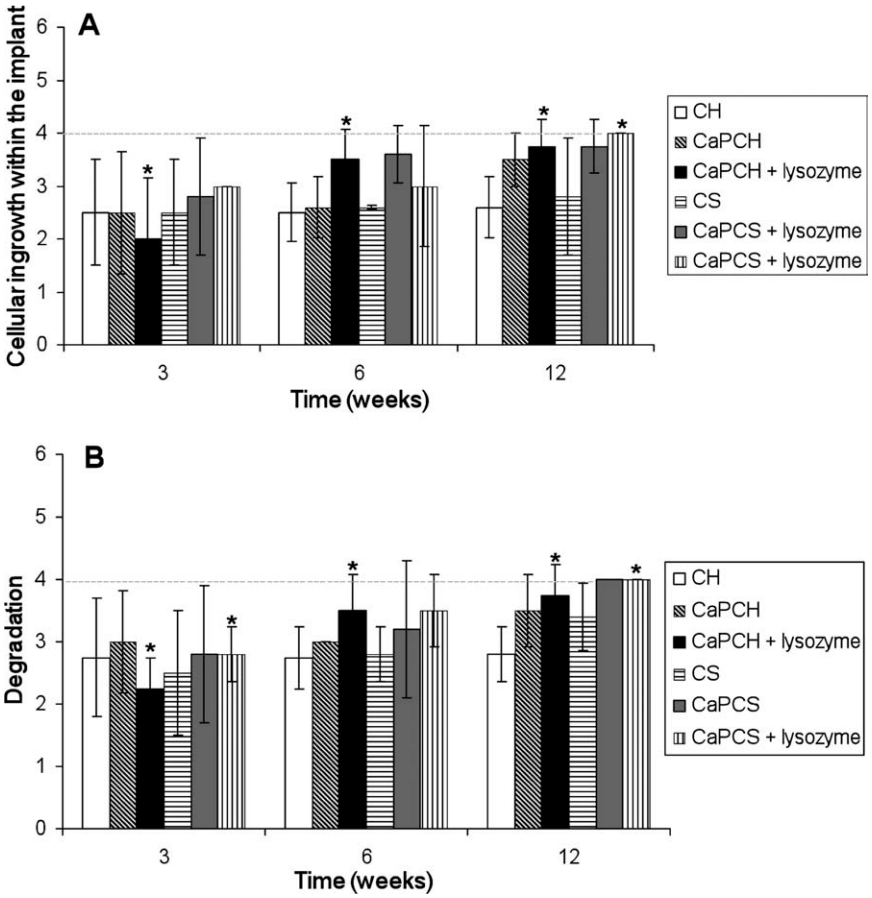

FIGURE 5. Results of histological scoring of: (A) cellular growth within the implants and (B) degradation after 3, 6, and 12 weeks of subcutaneous implantation. Data are presented as means ± standard deviation for $n = 4$–5. (*) indicates a significant difference ($p < 0.05$) between groups at the same time point.

32% after only 6 weeks (initial porosity of 9% ± 5% and 43% ± 7% after 6 weeks). The degradation and consequently the porosity is expected to be greater for longer implantation times. The pore interconnectivity of chitosan (CH) scaffolds significantly increased with increased implantation time when compared to the interconnectivity of control samples [Fig. 3(B)]. No significant differences in pore interconnectivity were observed between groups at the same time point. After 12 weeks all groups demonstrated a significant increase in pore interconnectivity with the exception of chitosan/starch scaffolds and CaPCS + lysozyme. Lysozyme seems to have no effect on pore interconnectivity; however, interconnectivity increased for all groups over time with a range of values from 24–31% and 43–79%, before and after 12 weeks implantation, respectively.

Microscopy analysis

Upon retrieval of the implants, no macroscopic signs of infection were observed at the surgical sites. Furthermore, no adverse tissue reactions (toxic effects) were observed with light microscopy. Specimens for microscopy were retrieved at 3, 6, and 12 weeks postimplantation. Polymer and CaP coating degradation, cellular ingrowth within the implants, as well as tissue response were assessed using histological techniques. Remaining scaffolds were easily identified after H&E staining, as chitosan and chitosan/starch stained red, and cells stained blue and pink. In Figure 4, CaP coatings are not easily identified (appear in dark blue/black), but to specifically stain calcium, several sections were stained with von Kossa (Fig. 6). For almost all scaffold formulations, the formation of pores and the infiltration of cells throughout the scaffolds (clearly visible at high magnifications) were evident, indicating material degradation and interconnectivity of the pores (Fig. 4). Degradation of scaffolds within the initially almost nonporous network of chitosan or chitosan/starch is evident through the presence of circular or irregular structures (pores) filled with cells (Fig. 4). Furthermore, as a function of implantation time, scaffolds have changed their shape and size, meaning that the scaffolds have been partially degraded and resorbed (Fig. 4). The infiltration of cells as a function of time is clearly visible [Fig. 5(A)] and occurred mainly when lysozyme was present. The progression of *in vivo* degradation was also evident by the qualitative observation of the formation of pores (Fig. 4). The increased scoring of degradation, especially when lysozyme was present, corroborated these data [Fig. 5(B)]. The degradation of scaffolds did not elicit a severe inflammatory response. For the success of a

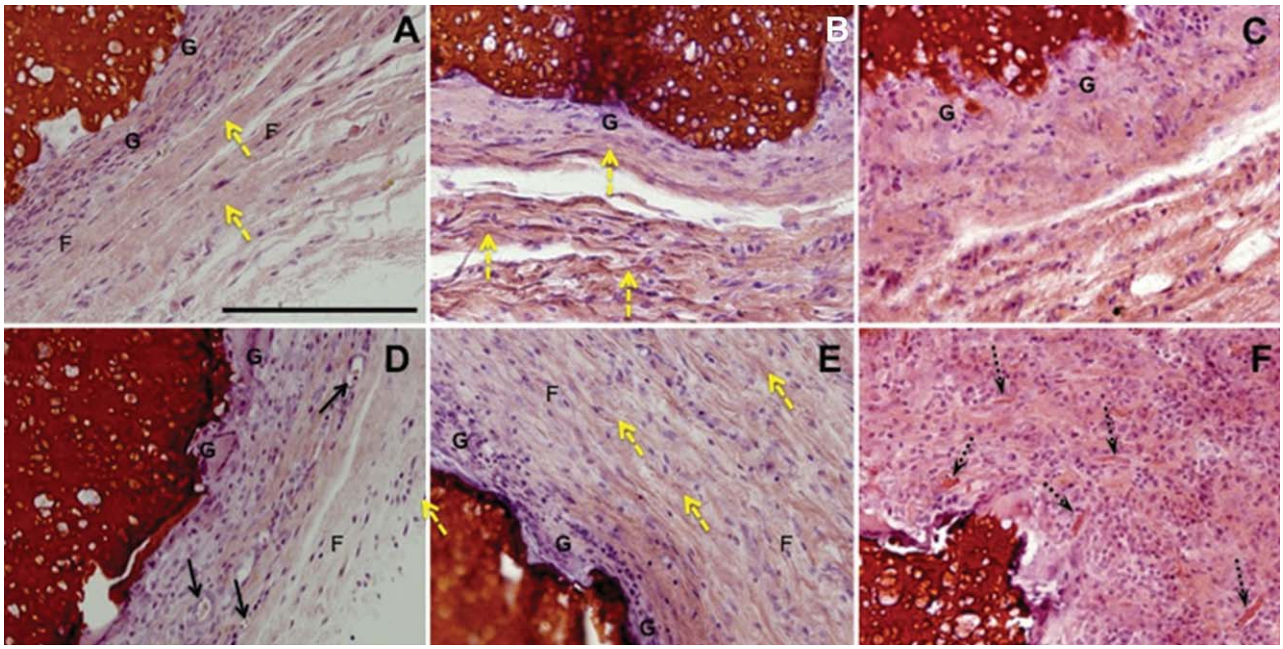

FIGURE 6. Representative light microscope images of the observed tissue responses at the implant interfaces. Chitosan/starch scaffolds (A–C) and CaP chitosan/starch scaffolds with incorporated lysozyme (D-F) stained with H&E after 3 (A, D), 6 (B, E), and 12 weeks (C, F) after subcutaneous implantation. Yellow arrows correspond to collagen deposits; black arrows represent blood vessels; dashed black arrows indicate scaffold fragments inside giant cells; G, giant cells; F, fibroblasts. The images are presented at 20× magnification. The scale bar is 200 μm and applies to all images. [Color figure can be viewed in the online issue, which is available at wileyonlinelibrary.com.]

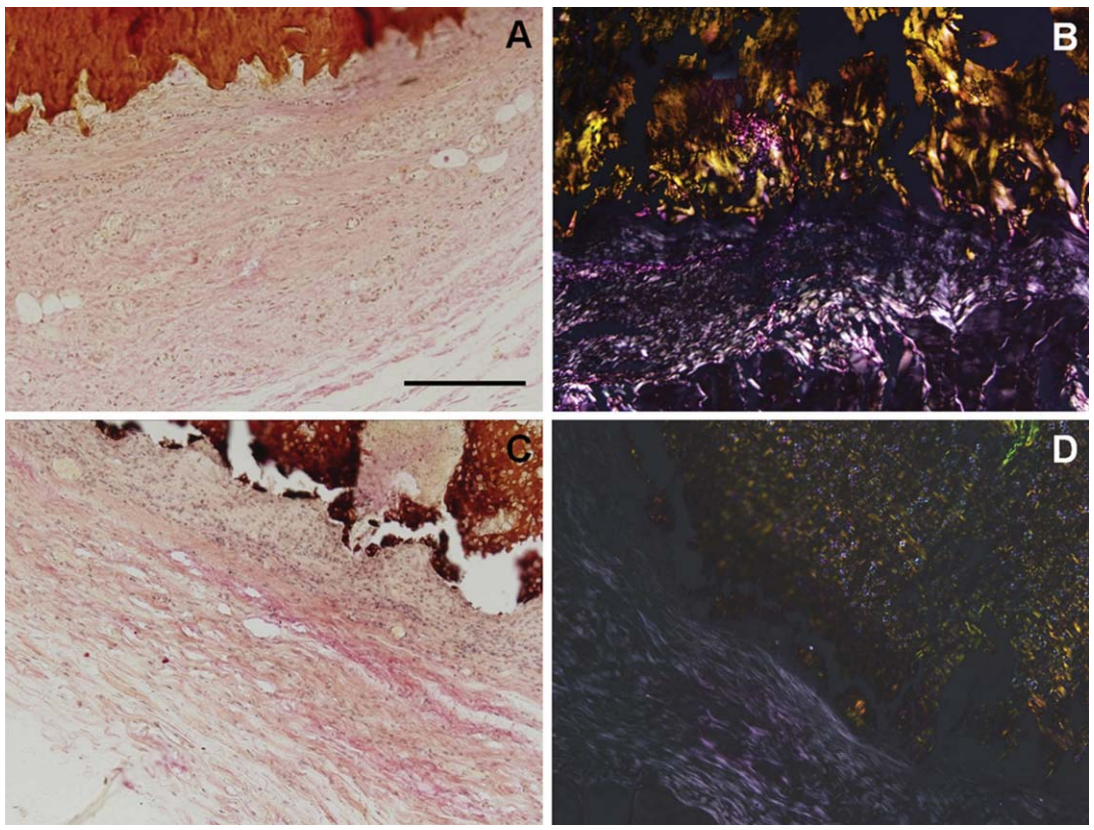

FIGURE 7. Representative images of van Gieson staining (A and C) and polarized light micrographs (B and D) of tissue surrounding chitosan (A and B) and CaPCH with incorporated lysozyme scaffolds (C and D) after 6 weeks of implantation. The images are presented at 10× magnification. The scale bar is 200 μm and applies to all images. [Color figure can be viewed in the online issue, which is available at wileyonlinelibrary.com.]

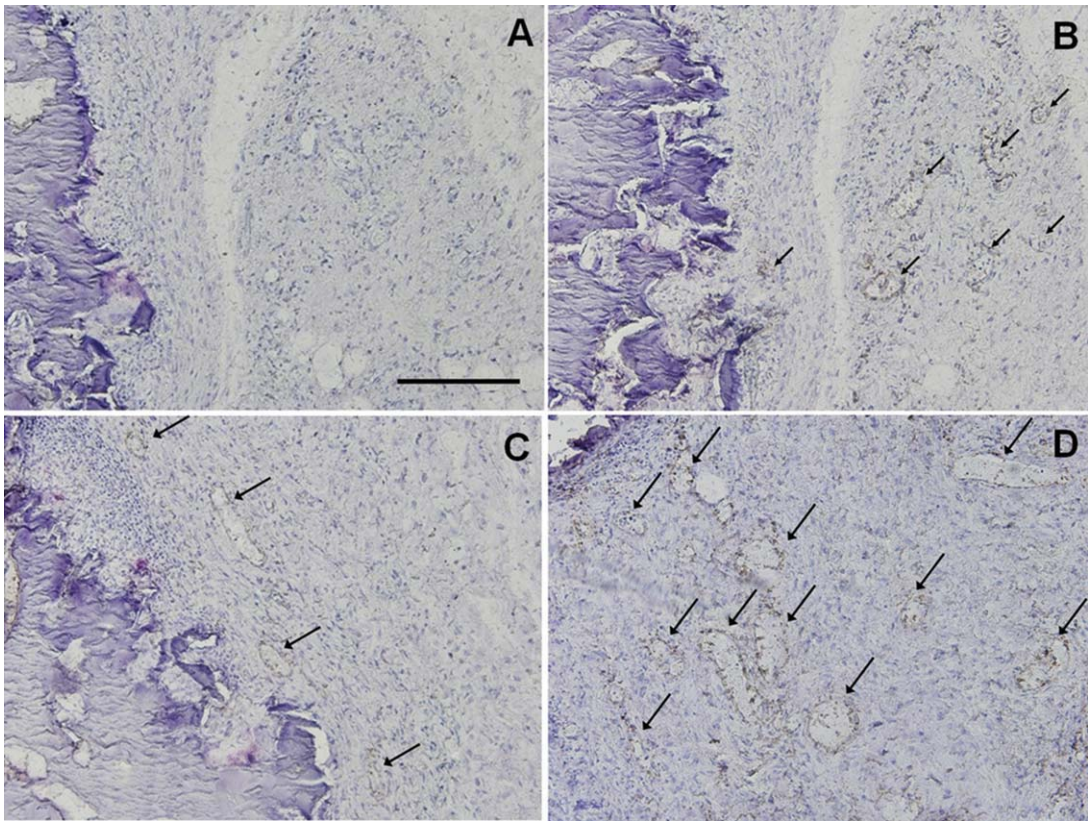

FIGURE 8. Representative α-SMA immunostaining images of tissue surrounding CaPCH with incorporated lysozyme after 3 and 6 weeks (B and C) and CaPCS after 12 weeks of implantation (D). Negative control (A). Arrows indicate blood vessels. The images are presented at 10× magnification. The scale bar is 200 μm and applies to all images. [Color figure can be viewed in the online issue, which is available at wileyonlinelibrary.com.]

bone tissue engineering implant, the scaffold must have a rate of degradation that corresponds to the rate of new bone ingrowth. The present strategy of *in situ* pore formation seems to have the potential to allow for a gradual transfer of mechanical support from the initial almost nonporous material to the tissue as a function of pore formation/scaffold degradation.

Biocompatibility is defined as "the ability of a material to perform with an appropriate host response in a specific situation."[33] The implantation of a biomaterial initiates a sequence of events starting with an acute inflammatory response and leading, in some cases, to a chronic inflammatory response and/or granulation tissue development, a foreign body reaction and fibrous capsule development.[34,35] In the literature, it is indicated that the intensity of the tissue response may be modulated by the biodegradation process, which in turn may be related with shape, porosity, surface roughness changes, formation of particulates, and release of degradation products.[34]

After 3 weeks of implantation, it was possible to observe macrophages, small blood vessels, fibroblasts, and some collagen [Fig. 6(A,D)]. After 6 weeks, the proliferation of fibroblasts and collagen fibrils become more abundant [Figs. 6(B,E) and 7] as well as multinuclear (giant cells) [Fig. 6(B,E)]. Collagen was visible even after 3 weeks [Fig. 6(A)] although after 6 weeks collagen deposition was more pronounced for all group conditions [Fig. 6(B,E)]. Collagen deposition was further confirmed by van Gieson staining and polarized light microscopy (Fig. 7). Furthermore, newly generated blood vessels were observed in the proximity of the implants [Fig. 6(D)]. The vascularization already observed in earlier times of implantation increased as the α-SMA labeling shows the newly formed blood vessels (Fig. 8). The density of vascularization increased as a function of implantation time (Fig. 8).

Foreign body reaction with granulation tissue is considered the normal wound healing response to implanted biomaterials.[35] Foreign body giant cells, implicated in the biodegradation of polymeric biomaterials,[35] were detected after 3 and 6 weeks [Fig. 6(A,B,D,E)] and increased after 12 weeks of implantation [Fig. 6(C,F)]. The foreign body reaction is composed of foreign body giant cells and the components of granulation tissue, such as, macrophages, fibroblasts, and capillaries in varying amounts.[35] The foreign body reaction consisting mainly of macrophages and/or foreign body giant cells may persist at the tissue-implant interface for the lifetime of the implant.[35] In the case of biodegradable polymers, the foreign body reaction will in general become persistent until final degradation is achieved.[36] It was observed that the number of macrophages and giant cells increased as a function of time (Fig. 6) to attempt to phagocytose the implanted materials.

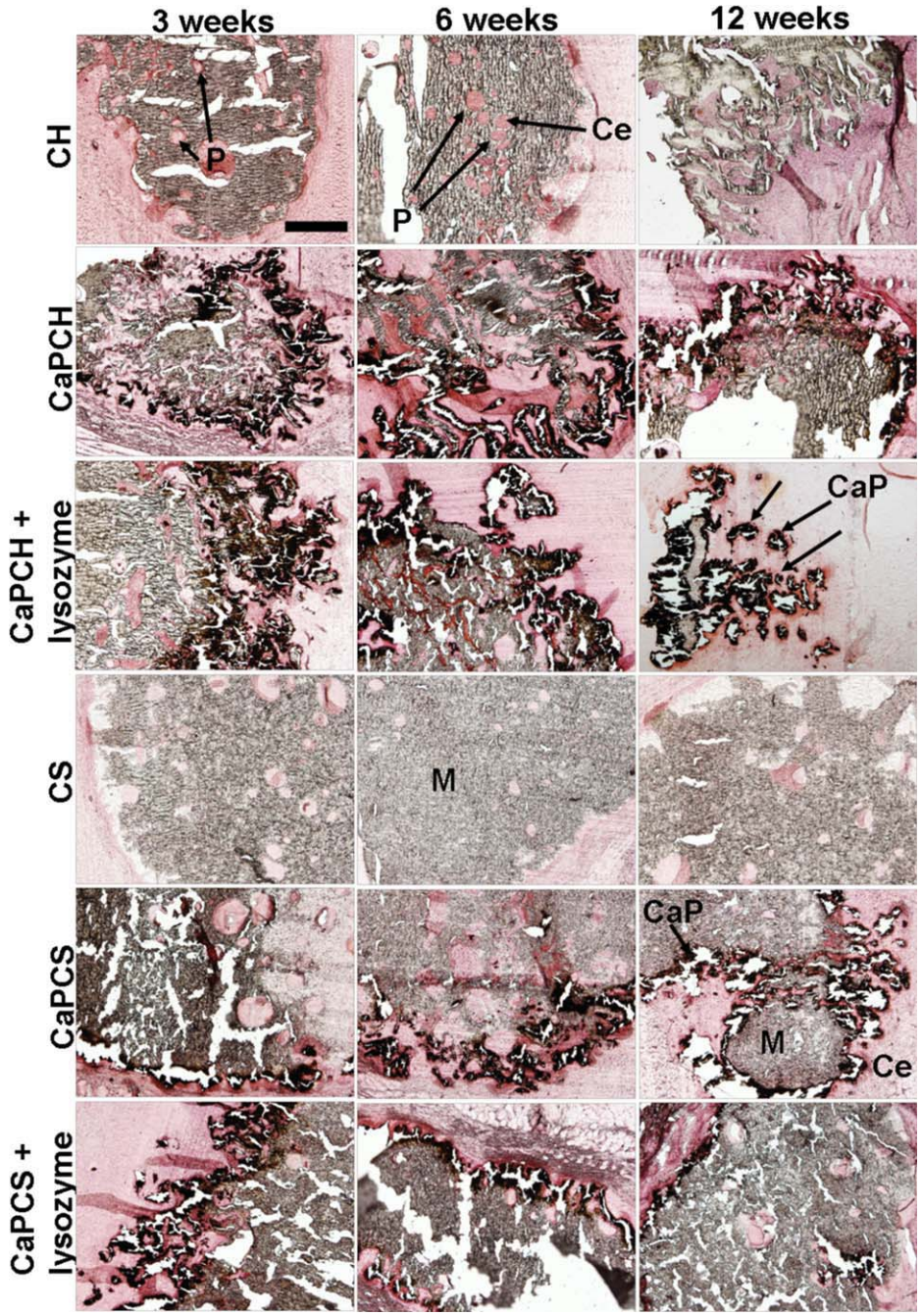

FIGURE 9. Representative light microscope images of chitosan-based sections stained with von Kossa after 3, 6, and 12 weeks of subcutaneous implantation. The images are presented at 4× magnification. The scale bar is 500 μm and applies to all images. Chitosan-based scaffolds (M) are stained in gray. Pores (P) are filled with cells (Ce) and appear in pink. CaP coatings (CaP) appear in black. [Color figure can be viewed in the online issue, which is available at wileyonlinelibrary.com.]

The interface between material and surrounding tissue at 12 weeks consisted in fibrin, macrophages and foreign body giant cells [Fig. 6(F)]. At the same time point, most scaffold formulations presented signs of degradation, as represented in Figure 6(F) where small fragments of material have been phagocytosed by giant cells. It was reported a similar behavior of 6 months implanted poly(D,L-lactide-caprolactone) with biomaterial particles engulfed inside giant cells.[37] Degradation of these materials can also interfere with wound healing. After 12 weeks healing tissue becomes unorganized with an increase of inflammatory cells and this can be attributed to degradation of the implanted materials, mainly when lysozyme was present [Fig. 6(F)]. The persistence of resident inflammatory cells may indicate that when lysozyme is present, the materials are undergoing active biodegradation. These materials did not induce a severe or abnormal inflammatory reaction at all studied implantation times. Although characterization of the specific types and

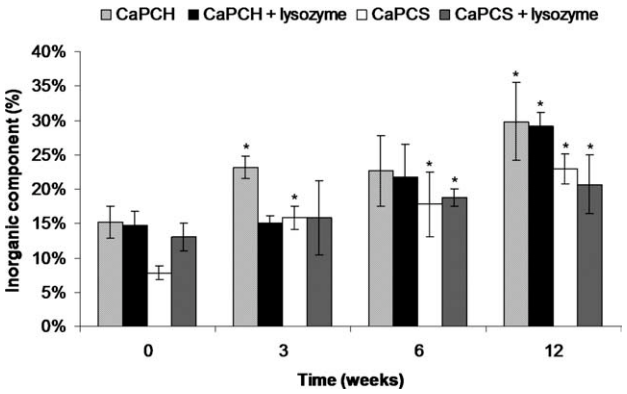

FIGURE 10. Quantification of mineral/inorganic component of chitosan-based scaffolds preimplantation and after 3, 6, and 12 weeks of implantation determined by TGA analysis. Data are presented as means ± standard deviation for $n = 3$. (*) indicates a significant difference ($p < 0.05$) at different time points compared with the control (0 weeks) for the same condition.

numbers of cells recruited to the constructs was beyond the scope of the present study, such characterization in future studies may elucidate the potential role of the CaP coatings and the presence of the released lysozyme on the overall inflammatory response of the host and the potential consequent effects on mineral turnover and bone deposition.

The principle of the biomimetic route is to immerse a substrate into simulated body fluid, favoring the nucleation and growth of bone-like apatite under physiological conditions of temperature and pH.[38] When a bioactive material is implanted, one of the first events is an ionic exchange between the CaP in contact with body fluids.[39] The dissolution leads to an increase of supersaturation at the surrounding area of the implant and afterwards to a precipitation onto the substrate of a bone-like carbonate apatite structure.[39–41] During resorption, the degradation products of CaP coatings (calcium and phosphate ions) are naturally metabolized and do not induce abnormal calcium and phosphate levels in urine, serum, or organs.[42,43] The dissolution of CaP coatings depends on the particle size, crystallographic features, density and the nature of the solution used to make the coating (composition, pH, and temperature).[43,44] These CaP coatings are partially amorphous and quite stable at pH 7.4.[2] Figure 9 shows von Kossa stained sections with CaP coating on or within the implants. The material is stained in gray, cells in pink, and CaP coating in black. All sections, with the exception of the controls (without CaP coatings), have black regions around or within the implants, meaning that the CaP coating did not dissolve completely. Signs of degradation of CaP coating were also evident in Figure 9. However, the coatings did not disappear *in vivo* but significantly increased. These results are corroborated by 3D images obtained by μ-CT (Fig. 2) and results obtained by TGA (Fig. 10). It was also possible to investigate the role of body fluids without the influence of bone cells, since these coated materials were tested subcutaneously in rats. TGA allowed quantification of the amount of mineral present on scaffolds preimplantation and indicated an increase in inorganic component with implantation time and for all coated conditions (Fig. 10). Furthermore, the amount of mineral significantly increased after 6 weeks for chitosan/starch scaffolds (CaPCS and CaPCS + lysozyme). The same trend was observed after 12 weeks for all groups with a significant increase in the mineral/inorganic component compared to that detected before implantation. The obtained results suggest a calcification/precipitation of the coating by mineral ions contained in the surrounding body fluid. This phenomenon was also observed in previous studies developed by Barrère et al.[39] We can state that in *in vivo* conditions the pH was mostly kept above 5 since the herein studied biomimetic CaP coatings are soluble at and below pH 5, as previously demonstrated.[2] Some studies showed improvement in the stability of the bone-bonding interface, at late implantation times of nonsoluble and stable CaP coated materials.[45,46] von Kossa stained sections also support the H&E results and histological scoring showing pronounced implant degradation as a function of implantation time and infiltration of cells throughout the implants (Figs. 5, 6, and 9).

CONCLUSIONS

In this study, the pore formation and *in vivo* degradation of chitosan-based materials, as well as the tissue response to the materials, were analyzed. The results demonstrated weight loss and increased porosity of the materials in a rat subcutaneous implantation model. Moreover, H&E staining of the sections obtained at different time points showed pores completely filled with cells, signifying that largely solid scaffolds were able to degrade, form pores and consequently be colonized by cells. Furthermore, μ-CT results corroborated these findings, showing that porosity significantly increased after 12 weeks of implantation, ranging from 22% up to 32% for all conditions, and that the pores are interconnected. This strategy, using biodegradable naturally occurring polymers such as chitosan and starch, seems to maintain structural support throughout the implantation period tested, with the formation of pores *in situ* allowing for the penetration of cells into the implants with a normal and mild inflammatory response by the host in a subcutaneous site. The gradual *in situ* pore forming ability of chitosan-based scaffolds was clearly demonstrated confirming the concept *in vivo*. This approach for *in situ* pore formation may have a lasting in bone tissue engineering by enabling gradual introduction of porosity into a scaffold *in vivo* to allow for tissue infiltration and load transfer to the tissue as a function of implantation time.

ACKNOWLEDGMENTS

We acknowledge Prof. Ademar Longatto, Luís Martins, Goreti Pinto, and Deolinda Teixeira (ICVS/3B's -Life and Health Sciences Research Institute - University of Minho, Portugal) for excellent technical assistance on histological sectioning and microscopy analysis; and also to Dr. Ricardo Silva for helping on TGA data analysis.

REFERENCES

1. Martins AM, Santos MI, Azevedo HS, Malafaya PB, Reis RL. Natural origin scaffolds with in situ pore forming capability for bone tissue engineering applications. Acta Biomater 2008;4:1637–1645.
2. Martins AM, Pereira RC, Leonor IB, Azevedo HS, Reis RL. Chitosan scaffolds incorporating lysozyme into CaP coatings produced by a biomimetic route: A novel concept for tissue engineering combining a self-regulated degradation system with in situ pore formation. Acta Biomater 2009;5:3328–3336.
3. Martins AM, Pham QP, Malafaya PB, Raphael RM, Kasper FK, Reis RL, Mikos AG. Natural stimulus responsive scaffolds/cells for bone tissue engineering: Influence of lysozyme upon scaffold degradation and osteogenic differentiation of cultured marrow stromal cells induced by CaP coatings. Tissue Eng Part A 2009;15: 1953–1963.
4. Martins AM, Salgado AJ, Azevedo HS, Leonor IB, Reis RL. Lysozyme incorporation in biomimetic coated chitosan scaffolds: Development and behaviour in contact with osteoblastic-like cells. Tissue Eng 2006;12:1018–1019.
5. Reis RL, Cunha AM, Fernandes MH, Correia RN. Treatments to induce the nucleation and growth of apatite-like layers on polymeric surfaces and foams. J Mater Sci Mater Med 1997;8: 897–905.
6. Oliveira AL, Elvira C, Reis RL, Vazquez B, San Roman J. Surface modification tailors the characteristics of biomimetic coatings nucleated on starch-based polymers. J Mater Sci Mater Med 1999;10:827–835.
7. Oliveira AL, Malafaya PB, Reis RL. Sodium silicate gel as a precursor for the in vitro nucleation and growth of a bone-like apatite coating in compact and porous polymeric structures. Biomaterials 2003;24:2575–2584.
8. Habibovic P, de Groot K. Osteoinductive biomaterials—Properties and relevance in bone repair. J Tissue Eng Regen Med 2007;1: 25–32.
9. Liu Y, Hunziker EB, Layrolle P, De Bruijn JD, De Groot K. Bone morphogenetic protein 2 incorporated into biomimetic coatings retains its biological activity. Tissue Eng 2004;10:101–108.
10. Azevedo HS, Leonor IB, Alves CM, Reis RL. Incorporation of proteins and enzymes at different stages of the preparation of calcium phosphate coatings on a degradable substrate by a biomimetic methodology. Mater Sci Eng C: Biomimetic Supramol Sys 2005;25:169–179.
11. Oliveira JM, Rodrigues MT, Silva SS, Malafaya PB, Gomes ME, Viegas CA, Dias IR, Azevedo JT, Mano JF, Reis RL. Novel hydroxyapatite/chitosan bilayered scaffold for osteochondral tissue-engineering applications: Scaffold design and its performance when seeded with goat bone marrow stromal cells. Biomaterials. 2006;27:6123–6137.
12. Malafaya PB, Santos TC, van Griensven M, Reis RL. Morphology, mechanical characterization and in vivo neo-vascularization of chitosan particle aggregated scaffolds architectures. Biomaterials 2008;29:3914–3926.
13. Costa-Pinto AR, Salgado AJ, Correlo VM, Sol P, Bhattacharya M, Charbord P, Reis RL, Neves NM. Adhesion, proliferation, and osteogenic differentiation of a mouse mesenchymal stem cell line (BMC9) seeded on novel melt-based chitosan/polyester 3D porous scaffolds. Tissue Eng Part A 2008;14:1049–1057.
14. Mendes SC, Reis RL, Bovell YP, Cunha AM, van Blitterswijk CA, de Bruijn JD. Biocompatibility testing of novel starch-based materials with potential application in orthopaedic surgery: A preliminary study. Biomaterials 2001;22:2057–2064.
15. Marques AP, Reis RL, Hunt JA. The biocompatibility of novel starch-based polymers and composites: In vitro studies. Biomaterials 2002;23:1471–1478.
16. Salgado AJ, Coutinho OP, Reis RL, Davies JE. In vivo response to starch-based scaffolds designed for bone tissue engineering applications. J Biomed Mater Res A 2007;80:983–989.
17. Azevedo HS, Gama FM, Reis RL. In vitro assessment of the enzymatic degradation of several starch based biomaterials. Biomacromolecules 2003;4:1703–1712.
18. Gomes ME, Azevedo HS, Moreira AR, Ella V, Kellomaki M, Reis RL. Starch-poly(epsilon-caprolactone) and starch-poly(lactic acid) fibre-mesh scaffolds for bone tissue engineering applications: Structure, mechanical properties and degradation behaviour. J Tissue Eng Regen Med 2008;2:243–252.
19. Tuzlakoglu K, Alves CM, Mano JF, Reis RL. Production and characterization of chitosan fibers and 3D fiber mesh scaffolds for tissue engineering applications. Macromol Biosci 2004;4:811–819.
20. Pham QP, Kasper FK, Mistry AS, Sharma U, Yasko AW, Jansen JA, Mikos AG. Analysis of the osteoinductive capacity and angiogenicity of an in vitro generated extracellular matrix. J Biomed Mater Res A 2009;88:295–303.
21. Young S, Patel ZS, Kretlow JD, Murphy MB, Mountziaris PM, Baggett LS, Ueda H, Tabata Y, Jansen JA, Wong M, Mikos AG. Dose effect of dual delivery of vascular endothelial growth factor and bone morphogenetic protein-2 on bone regeneration in a rat critical-size defect model. Tissue Eng Part A 2009;15:2347–2362.
22. Yoshikawa T, Ohgushi H, Akahane M, Tamai S, Ichijima K. Analysis of gene expression in osteogenic cultured marrow/hydroxyapatite construct implanted at ectopic sites: A comparison with the osteogenic ability of cancellous bone. J Biomed Mater Res. 1998;41: 568–573.
23. Nishikawa M, Myoui A, Ohgushi H, Ikeuchi M, Tamai N, Yoshikawa H. Bone tissue engineering using novel interconnected porous hydroxyapatite ceramics combined with marrow mesenchymal cells: Quantitative and three-dimensional image analysis. Cell Transplant 2004;13:367–376.
24. Uemura T, Dong J, Wang Y, Kojima H, Saito T, Iejima D, Kikuchi M, Tanaka J, Tateishi T. Transplantation of cultured bone cells using combinations of scaffolds and culture techniques. Biomaterials 2003;24:2277–2286.
25. Oliveira JM, Kotokuki N, Tadokoro M, Hirose M, Mano JF, Reis RL, Ohgushi H. Ex vivo culturing of rat bone marrow stromal cells with dexamethasone-loaded carboxymethylchitosan/poly(amidoamine) dendrimer nanoparticles enhances ectopic bone formation on tissue engineered constructs. Bone 2010;46:1424–1435.
26. Datta N, Holtorf HL, Sikavitsas VI, Jansen JA, Mikos AG. Effect of bone extracellular matrix synthesized in vitro on the osteoblastic differentiation of marrow stromal cells. Biomaterials. 2005;26: 971–977.
27. De Jong WH, Eelco Bergsma J, Robinson JE, Bos RR. Tissue response to partially in vitro predegraded poly-L-lactide implants. Biomaterials 2005;26:1781–1791.
28. Hankiewicz J, Swierczek E. Lysozyme in human body fluids. Clin Chim Acta 1974;57:205–209.
29. Porstmann B, Jung K, Schmechta H, Evers U, Pergande M, Porstmann T, Kramm HJ, Krause H. Measurement of lysozyme in human body fluids: Comparison of various enzyme immunoassay techniques and their diagnostic application. Clin Biochem 1989; 22:349–355.
30. Tomihata K, Ikada Y. In vitro and in vivo degradation of films of chitin and its deacetylated derivatives. Biomaterials 1997;18: 567–575.
31. Lim SM, Song DK, Oh SH, Lee-Yoon DS, Bae EH, Lee JH. In vitro and in vivo degradation behavior of acetylated chitosan porous beads. J Biomater Sci Polym Ed 2008;19:453–466.
32. Junge W, Troge B, Klein G, Poppe W, Gerber M. Evaluation of a new assay for pancreatic amylase: Performance characteristics and estimation of reference intervals. Clin Biochem 1989;22: 109–114.
33. Williams DF. On the mechanisms of biocompatibility. Biomaterials 2008;29:2941–2953.
34. Babensee JE, Anderson JM, McIntire LV, Mikos AG Host response to tissue engineered devices. Adv Drug Delivery Rev 1998;33: 111–139.
35. Anderson JM. Biological responses to materials. Ann Rev Mater Res 2001;31:81–110.
36. Luttikhuizen DT, van Amerongen MJ, de Feijter PC, Petersen AH, Harmsen MC, van Luyn MJA. The correlation between difference in foreign body reaction between implant locations and cytokine and MMP expression. Biomaterials 2006;27:5763–5770.
37. denDunnen WFA, Robinson PH, vanWessel R, Pennings AJ, vanLeeuwen MBM, Schakenraad JM. Long-term evaluation of degradation and foreign-body reaction of subcutaneously implanted poly(DL-lactide-epsilon-caprolactone). J Biomed Mater Res 1997;36: 337–346.

38. Abe Y, Kokubo T, Yamamuro T. Apatite coating on ceramics: Metals and polymers utilizing a biological process. J Mater Sci: Mater Med 1990;1:233–238.
39. Barrere F, van der Valk CM, Dalmeijer RA, van Blitterswijk CA, de Groot K, Layrolle P. In vitro and in vivo degradation of biomimetic octacalcium phosphate and carbonate apatite coatings on titanium implants. J Biomed Mater Res A 2003;64:378–387.
40. Heughebaert M, LeGeros RZ, Gineste M, Guilhem A, Bonel G. Physicochemical characterization of deposits associated with HA ceramics implanted in nonosseous sites. J Biomed Mater Res Appl Biomater 1988;22:257–268.
41. Radin SR, Ducheyne P. The effect of calcium phosphate ceramic composition and structure on in vitro behavior. II. Precipitation. J Biomed Mater Res 1993;27:35–45.
42. den Hollander W, Patka P, Klein CP, Heidendal GA. Macroporous calcium phosphate ceramics for bone substitution: A tracer study on biodegradation with 45Ca tracer. Biomaterials 1991;12: 569–573.
43. Barrere F, van Blitterswijk CA, de Groot K. Bone regeneration: Molecular and cellular interactions with calcium phosphate ceramics. Int J Nanomedicine 2006;1:317–332.
44. Leeuwenburgh SC, Wolke JG, Siebers MC, Schoonman J, Jansen JA. In vitro and in vivo reactivity of porous, electrosprayed calcium phosphate coatings. Biomaterials 2006;27:3368–3378.
45. Dhert WJ, Klein CP, Jansen JA, van der Velde EA, Vriesde RC, Rozing PM, de Groot K. A histological and histomorphometrical investigation of fluorapatite, magnesiumwhitlockite, and hydroxylapatite plasma-sprayed coatings in goats. J Biomed Mater Res 1993;27:127–138.
46. Klein CP, Wolke JG, de Blieck-Hogervorst JM, de Groot K. Calcium phosphate plasma-sprayed coatings and their stability: An in vivo study. J Biomed Mater Res 1994;28:909–917.